JCTC Journal of Chemical Theory and Computation

ARTICLE

pubs.acs.org/JCTC

# A Qualitative Index of Spatial Extent in Charge-Transfer Excitations

Tangui Le Bahers,* Carlo Adamo, and Ilaria Ciofini*

LECIME, Laboratoire d'Electrochimie, Chimie des Interfaces et Modélisation pour l'Energie, CNRS UMR-7575, Ecole Nationale Supérieure de Chimie de Paris—Chimie ParisTech, 11 rue P. et M. Curie, 75231 Paris Cedex 05, France

Supporting Information

**ABSTRACT:** With the aim of defining the spatial extent associated to an electronic transition, of particular relevance in the case of charge-transfer (CT) excitations, a new index, evaluated only from the computed density for the ground and excited state, is here derived and tested on a family of molecules that can be considered as prototypes of push—pull chromophores.The index ($D_{CT}$) allows to define the spatial extent associated to a given transition as well as the associated fraction of electron transferred. By definition of centroids of charges associated to the density increase and depletion zones upon excitation, a qualitative and easy to visualize measure of the spatial extent of the donor and the acceptor moieties within a given molecular system is also given. Finally, an index ($t$) allowing to define the presence eventually pathologic CT transitions for time-dependent density functional theory treatment in conjunction with standard generalized gradient approximation or hybrid functional, that is through space CT, is disclosed.

## 1. INTRODUCTION

Push—pull systems made up of an electron donor (D) and an electron withdrawing (A) groups covalently connected are one of the most pursued families of compounds when aiming at obtaining intense—and solvatochromic—optical transitions in the visible spectral region.[1] The latter are basically associated to the formation of an excited state corresponding to the transfer of an electron from the donor to the acceptor, that is to the formation of a $[D^+—A^-]^*$ excited state.[2]

Clearly, this simple representation of the excited state and of the electron transfer process is modulated and strongly depends both on the type of chemical link present between the donor and the acceptor subunits (normally defined as spacer) and on their intrinsic nature.

In most of the real cases, both the length and the magnitude of the electron transfer due to the excitation are far from ideal (that is one electron transferred from the donor and localized on the acceptor).[3] Depending on the intramolecular geometrical and electronic coupling, the transferred electron is, in some cases, delocalized from the region of the molecule nearby the donor to one in the vicinity of the acceptor.[4]

This effect can be qualitatively inspected by the analysis of the density distribution at the ground and the excited state.[5] Nevertheless, even regions of the molecule not presenting a net change in total density can show an alternation of excess and depletion of density as a consequence of the electronic transition, thus making difficult to use directly the density distribution maps to follow and quantify the charge-transfer (CT) phenomena.[5,6]

Obtaining a more quantitative measure of the length and magnitude of the CT is far from trivial both from the experimental and the theoretical point of view.

At the theoretical level, quantifying the magnitude of the charge transferred on a given spatial region implies to transform the known electron distribution over space computed for the ground and excited states to a condensed, that is localized, index, therefore implying the use of a (arbitrary) localization scheme. Any measures derived in such a way will thus depend both on the model, level of theory, used to compute the excited and ground state densities and on the localization procedure applied.

The basic idea of the simple model here proposed is to define a measure of the length of a CT excitation solely on the basis of the total electronic density computed for the ground and excited states. This method is thus applicable to any quantum chemical method supplying densities for the ground and excited states, providing in principle a very simple way to qualitatively compare the outcomes of post-Hartee—Fock (HF) and density functional theory (DFT)-based approaches. To this end, the following steps will be considered:

- Definition of the barycenters of the density depletion and the density increment zones associated with the electronic transition and computed over a grid of points.
- Definition of the CT length as distance between the barycenters.
- Definition of the transferred charge by integration of the density depletion function over all space.
- Calculation of the associated dipole moment.

None of these steps is either time or resources demanding so that our method can be applied to screen and analyzed any kind of molecular system for which ground and excited densities on a grid can be computed. Furthermore, none of the previous steps requires defining a subdomain in the molecule, thus it does not introduce any arbitrary localization scheme.

Next, in order to provide a simple way to visualize the spatial extent of the transition, inspired by literature works aimed at giving a mathematical definition to the concept of size of an electron pair,[7,8] we propose to define two centroids of density corresponding to the density depletion and the density increment regions. A qualitative measure of the overlap between the

**Received:** May 4, 2011
**Published:** June 23, 2011

centroids is then used to quantify the through-space character associated to a computed CT excitation.

Overall, the model here developed is finally aimed to be used to qualitatively screen push−pull compounds belonging to different chemical families in terms of length and magnitude of charge transferred in order to provide useful insights for experimental chemists. Besides it can also be shown that a simple qualitative diagnostic index for through-space CT excitations, of interest at time dependent DFT (TD-DFT) level, may be easily derived.

The paper is organized as follows: After a description of the method (Section 2) and the computational details (Section 3), the results obtained at a fixed level of theory for a family of molecules experimentally characterized are discussed in Section 4. Finally, in Section 5 some general insights about the applicability of these indexes to identify pathological behavior of time-dependent (TD)-DFT for the treatment of through-space CT transitions are given.

## 2. THE MODEL

Defining $\rho_{GS}(r)$ and $\rho_{EX}(r)$ as the electronic densities associated to the ground and excited states, the density variation associated to the electronic transition is given by

$$\Delta\rho(r) = \rho_{EX}(r) - \rho_{GS}(r) \tag{1}$$

Two functions, $\rho_+(r)$ and $\rho_-(r)$, defining the points in space where an increment or a depletion of the density upon absorption is produced ($\Delta\rho(r)$) can be defined as follows:

$$\rho_+(r) = \begin{cases} \Delta\rho(r) & \text{if } \Delta\rho(r) > 0 \\ 0 & \text{if } \Delta\rho(r) < 0 \end{cases} \tag{2}$$

$$\rho_-(r) = \begin{cases} \Delta\rho(r) & \text{if } \Delta\rho(r) < 0 \\ 0 & \text{if } \Delta\rho(r) > 0 \end{cases} \tag{3}$$

The barycenters of the spatial regions defined by $\rho_+(r)$ and $\rho_-(r)$, referred in the following as $R_+$ and $R_-$, can thus be defined [for instance discretizing it on a three-dimensional (3D) grid around the molecule] as

$$R_+ = \frac{\int r\rho_+(r)\mathrm{d}r}{\int \rho_+(r)\mathrm{d}r} = (x_+, y_+, z_+) \tag{4}$$

$$R_- = \frac{\int r\rho_-(r)\mathrm{d}r}{\int \rho_-(r)\mathrm{d}r} = (x_-, y_-, z_-) \tag{5}$$

The spatial distance between the two barycenters of density distributions can thus be used to "measure" the CT excitation length $D_{CT}$ as

$$D_{CT} = |R_+ - R_-| \tag{6}$$

Integrating over all space $\rho_+$ ($\rho_-$), the transferred charge ($q_{CT}$) can be defined. For one electron excitation, $q_{CT}$ can assume values between 0 and 1. Analogously, a variation in dipole moment between the ground and the excited states ($\mu_{CT}$) can be defined, and its norm is computed by the following relation:

$$\left\|\mu_{CT}\right\| = D_{CT}\int \rho_+(r)\mathrm{d}r = -D_{CT}\int \rho_-(r)\mathrm{d}r$$
$$= D_{CT}q_{CT} \tag{7}$$

This value has to be identical to the difference between the dipole moments computed for the ground and the excited states, that is $\Delta\mu_{ES-GS}$. In order to lighten notations, the $\|\mu_{CT}\|$ term will be replaced in the following by $\mu_{CT}$.

For visualization purposes, it is also interesting to define two centroids of charges associated to the positive and negative density regions. To this end, first the root-mean-square deviations along the three axis ($\sigma_{aj}$, $j = x, y, z$; $a = +$ or $-$) are computed as

$$\sigma_{a,j} = \sqrt{\frac{\Sigma_i \rho_a(r_i)(j_i - j_a)^2}{\Sigma_i \rho_a(r_i)}} \tag{8}$$

The two centroids ($C_+$ and $C_-$) can then simply be defined as

$$C_+(r) = A_+ \mathrm{e}\left(-\frac{(x-x_+)^2}{2\sigma_{+x}^2} - \frac{(y-y_+)^2}{2\sigma_{+y}^2} - \frac{(z-z_+)^2}{2\sigma_{+z}^2}\right) \tag{9}$$

$$C_-(r) = A_- \mathrm{e}\left(-\frac{(x-x_-)^2}{2\sigma_{-x}^2} - \frac{(y-y_-)^2}{2\sigma_{-y}^2} - \frac{(z-z_-)^2}{2\sigma_{-z}^2}\right) \tag{10}$$

The normalization factors ($A_+$ and $A_-$) can be chosen so as to impose the integrated charge on the centroid to be equal to the corresponding density change integrated in the whole space:

$$A_+ = \frac{\int \rho_+(r)\mathrm{d}r}{\int \mathrm{e}\left(-\frac{(x-x_+)^2}{2\sigma_{+x}^2} - \frac{(y-y_+)^2}{2\sigma_{+y}^2} - \frac{(z-z_+)^2}{2\sigma_{+z}^2}\right)\mathrm{d}r} \tag{11}$$

$$A_- = \frac{\int \rho_-(r)\mathrm{d}r}{\int \mathrm{e}\left(-\frac{(x-x_-)^2}{2\sigma_{-x}^2} - \frac{(y-y_-)^2}{2\sigma_{-y}^2} - \frac{(z-z_-)^2}{2\sigma_{-z}^2}\right)\mathrm{d}r} \tag{12}$$

This definition has been used throughout in the present work. By definition this normalization imposes also the physical constrain that $\int\rho_-(r)\mathrm{d}r = -\int\rho_+(r)\mathrm{d}r$

For purposes of analysis of rod-like dyads, it may be of interest to define an index (named $H$) as half of the sum of the centroids axis along the $D-A$ direction. For instance, if the $D-A$ direction is along the $x$ axis, $H$ is defined by the relation:

$$H = \frac{\sigma_{+x} + \sigma_{-x}}{2} \tag{13}$$

For $H \geq D_{CT}$, an overlap between the centroids along this axis is thus expected.

Finally, the $t$ represents the difference between $D_{CT}$ and $H$:

$$t = D_{CT} - H \tag{14}$$

## 3. COMPUTATIONAL DETAILS

At the ground state, the structure of all systems was optimized at DFT level using the hybrid PBE0[9] functional and the 6-31+G(d) basis set.[10] All calculations were performed using the Gaussian package,[11] and bulk solvent (ethanol, EtOH) effects were taken into account using a continuum solvation model (C-PCM).[12,13] When not differently specified, vertical excitations energies and associated excited state densities were computed at TD-DFT at the same level of theory. Five excited states were computed for all systems analyzed. Using PBE0 ground-state structures, the first five excited states were also computed at CIS level and (using the TD-DFT approach) also using the Perdew, Burke, and Ernzerhof (PBE)[14] and LC-PBE[15] functional, always keeping the 6-31+G(d) basis set.

In this work, densities (for both the ground and the excited states) were computed on a grid of points using the cubegen utility (and associated default options) provided by the Gaussian package.[11] All density derived quantities were computed using numerical integration procedure by using internally developed software. The consistency of the size of the box used has been checked computing the net fraction of escaped electrons ($\delta_{esc}$), that is

$$\delta_{esc} = N - \int_{box} \rho^{box}(r)\mathrm{d}r \qquad (15)$$

where $N$ is the total number of electrons in the molecule and $\rho(r)$ is the total ground-state density.

## 4. A TEST CASE: A SIMPLE D-$\Pi$-A FAMILY OF MOLECULES

**4.1. Structural and Electronic Properties.** In order to test the performance of our index, we considered the family of molecules depicted in Figure 1, which can be considered as prototypes of donor−acceptor systems (dyads) expected to show a significant intramolecular CT character for the first excitation. In these molecules, spectroscopically characterized,[16] the length of CT from the donor (amino, $NH_2$ noted D) to the acceptor (nitro, $NO_2$ noted A) group is modulated by the presence of an increasing number of conjugated phenyl spacers ($\pi_n$, $n$ = 1−5). In the following these dyads will therefore be labeled as P$n$, where $n$ represents the number of phenyl spacers present in the molecule.

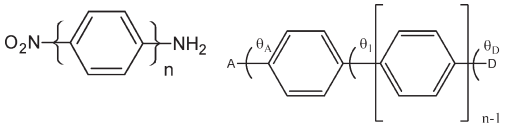


**Figure 1.** The family of molecules considered in the present work (right) and their labeling scheme (right), $n$ = 1−5.

The main structural parameters corresponding to the optimized structures at PBE0/6-31+G(d) level are reported in Table 1, while the computed excitation energies and oscillator strengths associated to the first five transitions are collected in Table 2. As can be noted all P$n$ molecules present a staggered conformation of the phenyl rings, with an inter-ring dihedral angle going from ca. 31° for the shortest molecules to ca. 35° for P$n$ systems with $n \geq 4$ and a practically constant carbon to carbon inter-ring bond (between 1.471 and 1.478 Å). The coupling of the donor and acceptor groups to the phenyl spacer, which is ruled both by the $N_x$−C distances and the $\Theta_x$ dihedral angles ($x$ = A, D), is also comparable for all the systems analyzed (Table 1). Therefore we can reasonably assume that from a purely geometrical point of view the same kind of coupling is present in all P$n$ systems and that the only relevant geometrical parameter is the increase in distance between the donor and acceptor units. In this respect, they constitute an ideal benchmark for our purposes.

The CT excitation for all systems corresponds basically to an one-electron highest occupied molecular orbital−lowest unoccupied molecular orbital (HOMO−LUMO) excitation. The computed vertical excitation energies (Table 2) are strongly underestimated at PBE0 level for all systems but P1. Only for P1, the error on computed transition energies (0.10 eV) is in line with what was expected at this level of theory when neglecting direct

**Table 2. Computed (PBE0/6-31+G(d)/PCM-EtOH) and Experimental Transition Energies (in nm) Associated to the First Excitation for the P$n$ Systems along with the Corresponding Computed Oscillator Strengths and Experimental $\varepsilon$ Values (in $M^{-1}\cdot cm^{-1}$ from ref 16)**

| $N$ | $\lambda_{calc}$ | $f_{calc}$ | $\lambda_{exp}$ | $\varepsilon_{exp}(10^{-4})$ |
|---|---|---|---|---|
| 1 | 362 | 0.65 | 372 (EtOH) | 1.68 |
| 2 | 460 | 0.69 | 377 (EtOH) | 1.38 |
| 3 | 483 | 0.54 | 358 (EtOH) | 1.65 |
| 4 | 478 | 0.38 | 340 (DMF) | 3.7 |
| 5 | 470 | 0.27 | – | – |

**Table 1. Computed (PBE0/6-31+G(d)/PCM-EtOH) Structural Parameters (angles in °, distances in Å) for the P$n$ Systems[a]**

| $n$ | $dN_DN_A$ | $\Theta_A$ $d(N_AC)$ | $\Theta_D$ $d(N_DC)$ | $\Theta_1$ $d(C-C)_1$ | $\Theta_2$ $d(C-C)_2$ | $\Theta_3$ $d(C-C)_3$ | $\Theta_4$ $d(C-C)_4$ | $\Theta_5$ $d(C-C)_5$ |
|---|---|---|---|---|---|---|---|---|
| 1 | 5.579 | 0.05 | −12.15 | – | – | – | – | – |
| | | 1.429 | 1.355 | | | | | |
| 2 | 9.933 | 0.37 | −23.82 | −31.23 | – | – | – | – |
| | | 1.447 | 1.380 | 1.471 | | | | |
| 3 | 14.262 | 0.47 | −25.27 | −33.83 | 33.31 | – | – | – |
| | | 1.451 | 1.386 | 1.475 | 1.476 | | | |
| 4 | 18.585 | 0.28 | −25.98 | −35.14 | 35.01 | −34.40 | – | – |
| | | 1.452 | 1.388 | 1.476 | 1.478 | 1.477 | | |
| 5 | 22.906 | 0.22 | −25.91 | −35.03 | 35.23 | −35.24 | 34.07 | – |
| | | 1.452 | 1.388 | 1.477 | 1.478 | 1.478 | 1.477 | |

[a] For labeling refer to Figure 1. The phenyl spacers are numbered going from A to D, $d(CC)_x$ distances represent the distance between carbon atoms belonging to the $x$ and $x$ + 1 phenyl groups.

solute solvent interactions (hydrogen bonding) that may be of importance in the case of EtOH.[17] Indeed, if a good spatial proximity between the donor (HOMO) and the acceptor (LUMO) orbitals is computed for P1 (Figure 2) starting from the P2 system, only a weak overlap can be evidenced between the donor and the acceptor units (Figure 2).

The very large errors on computed transition energies obtained for P*n* systems ($n$ = 2 to 5, Table 2) are thus not surprising, since the underestimation and the collapse of through-space CT transition energies when using TD-DFT with nonasymptotically corrected exchange correlation functionals or in absence of correction to the linear response approach is very well documented in literature (see for instance refs 18−31). Fixing to the standard LR-TD-DFT, the use of range separated functionals, such as LC-PBE should cure this problem although vertical excitation energies computed at this level of theory may not be quantitative agreement with experimental data.[32−36]

**4.2. CT Indexes at PBE0 Level.** In this paragraph the indexes obtained at PBE0 level will be discussed in order to show their potential interest for the description of the nature of the CT states. Indeed, the real nature of the excited states, which are better described using range-separated hybrids, will be discussed in the following sections.

Using the total density computed for the ground and excited states, it is possible to evaluate $\Delta\rho$, $\rho_+$, and $\rho_-$ on a grid of points around the molecule as defined by eqs 1−3. The density variation upon excitation ($\Delta\rho$), computed for the first electronic transition at PBE0 level, is graphically depicted in Figure 3, the green and red zones corresponding to $\rho_+$ and $\rho_-$, respectively.

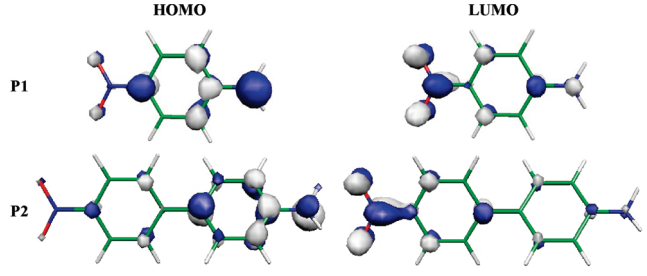


**Figure 2.** Computed (PBE0/6-31+G(d)/PCM)) HOMO and LUMO orbitals for the P1 (top) and P2 (bottom) systems. Isocontour value 0.005 au.

As expected the density depletion zones (red, Figure 3) are mostly located on the $NH_2$ donor group but actually quite delocalized on the phenyl(s) directly connected to it. This finding is consistent with a weak donor character of the phenyl ring. On the other hand the regions of density increment (green, Figure 3) look more localized on the acceptor moiety, formally corresponding to the nitro ($NO_2$) group and, only to a minor extent, to the phenyl ring directly connected to it.

The use of the barycenter of charge ($R_+$ and $R_-$, eqs 4 and 5) allows to quantify these qualitative observations. In fact, while the $R_-$ barycenter is very close to the $NO_2$ group (Figure 3) in the case of $R_+$ a displacement toward the phenyl rings closer to the amino group is clearly computed, thus highlighting their donor character.

As a consequence, the length of CT ($D_{CT}$) does not correspond to the distance between the donor and the acceptor groups ($d(N_AN_D)$) as clearly evident from the data collected in Table 3 and in Figure 4. In practice, due to the delocalization of mainly the donor group, while the physical distance between $A$ and $D$ increases ca. 4.33 Å for each phenyl unit added, the corresponding increase in $D_{CT}$ is only of ca. 2.36 Å. Indeed, the length of the CT, $D_{CT}$, increases more slowly than the distance $d(N_AN_D)$ when phenyl spacers are added. This results in an $A$ coefficient lower than 1 in Figure 4.

**Table 3. Computed (PBE0/6-31+G(d)/PCM-EtOH) Distances between Donor and Acceptor Groups ($d(N_D - N_A)$, in Å), Length, Charge and Dipole Moment ($D_{CT}$, $q_{CT}$ and $\mu_{CT}$ in Å, $|e^-|$ and Debye, respectively) Associated to the CT Excitation Together with the Computed Fraction of Escaped Electron ($\delta_{esc}$, in $|e^-|$) and the Difference between Ground- and Excited-State Dipole Moments ($\Delta\mu_{GS-ES}$, in Debye)[a]**

| | PBE0 | | | | | | |
|---|---|---|---|---|---|---|---|
| $N$ | $d(N_D-N_A)$ | $D_{CT}$ | $q_{CT}$ | $\mu_{CT}$ | $\Delta\mu_{GS-ES}$ | $\delta_{esc}$ | $H$ |
| 1 | 5.58 | 2.6 | 0.5 | 6.6 | 6.6 | 0.07 | 2.0 |
| 2 | 9.93 | 4.9 | $0.8_5$ | 20.1 | 20.1 | 0.06 | 3.1 |
| 3 | 14.26 | 7.2 | 1.0 | 36.4 | 36.4 | 0.00 | 4.3 |
| 4 | 18.59 | 9.5 | 1.2 | 52.9 | 53.0 | 0.04 | 5.4 |
| 5 | 22.91 | 11.9 | 1.2 | 69.9 | 69.9 | 0.17 | 6.6 |

[a] The last column ($H$, in Å) represents the half sum of the centroids axis length along the $D-A$ direction.

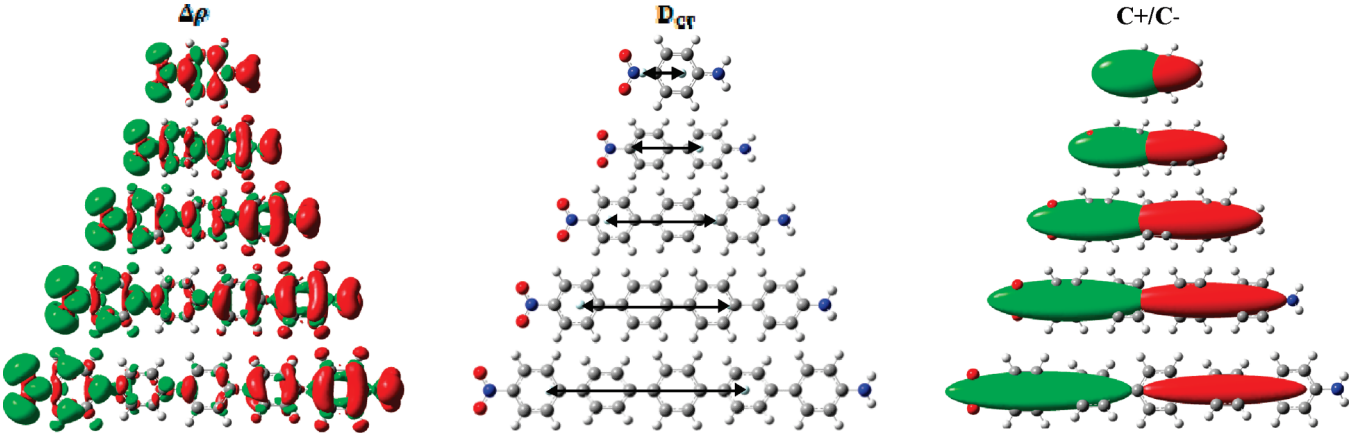


**Figure 3.** Computed (PBE0/6-31+G(d)/PCM)) difference in total density computed for the ground and excited states ($\Delta\rho(r) = \rho_{EX}(r) - \rho_{GS}(r)$, isocontour value 0.001 au), graphical representation of $D_{CT}$, and centroids of charge ($C_+(r)/C_-(r)$, isocontour value 0.001 au).

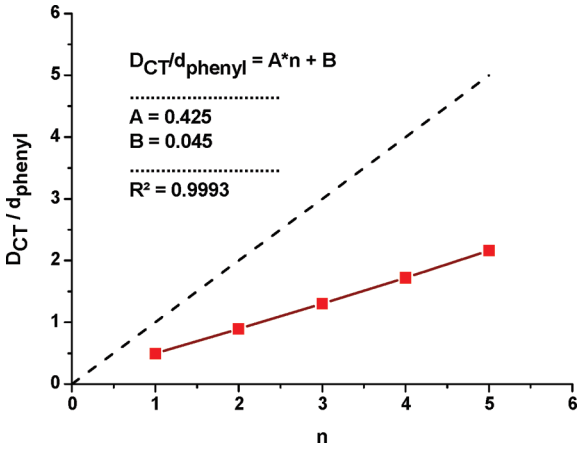


**Figure 4.** Normalized $D_{CT}$ ($D_{CT}/d_{phenyl}$, $d_{phenyl}$ being the average phenyl length set to 4.33 Å) as a function of the number of phenyl spacer, *n*.

By integration of $\rho_+$ ($\rho_-$) over all space, the transferred charge can be evaluated, and the numerical values are reported in Table 3. Clearly, if for the P1 system the transition has still a local character ($D_{CT}$ and $q_{CT}$ being only 2.5 Å and 0.5 $|e^-|$, respectively) the transition computed for the P2 dyad shows a net CT character, the computed $q_{CT}$ value being 0.8 $|e^-|$. Of note, for the larger systems (P4 and P5) unphysical, that is larger than 1, values of $q_{CT}$ (of the order of 1.2−1.3 $|e^-|$) are computed. This finding is related to the accuracy of the sampling of the density over a grid. As a matter of fact, the integration volume (box) chosen for these systems is too small, as demonstrated by the computed escaped density, which leads to 0.04−0.22 $|e^-|$ computed to be out of our integration grid ($\delta_{esc}$ in Table 3). The value of the escaped charge for the excited state is, in the present case, strictly equivalent to that computed for the ground state. The computed change in dipole moment between the ground and excited states is evaluated using either $D_{CT}$ and $q_{CT}$ by eq 7 ($\mu_{CT,}$ Table 3) or as expectation values over the density of the ground and excited states ($\Delta\mu_{GS-ES}$, Table 3) that are thus numerically equivalent. Nevertheless, in general cases particular care should be taken when using diffuse orbitals which may contribute more to the description of the excited states, thus determining a larger value for the escaped charge at the excited state.

It is worth noting that none of the quantities discussed up to now ($D_{CT}$, $q_{CT}$, and $\mu_{CT}$) depend on an arbitrary localization scheme but only on the quality of the density used for the ground and the excited state. Therefore, they could be used to fairly compare different levels of theory used to evaluate the ground- and excited-state densities. This point will be addressed in the next section.

In order to visualize the spatial extent and the overlap between the regions of density depletion and increment, two centroids of charge have been defined using eq 9 and 10. The computed centroids are reported in Figure 3. Using this arbitrarily condensed function, on one hand, it is much easier to identify the spatial extent of the "real" donor and acceptor moieties and, on the other hand, to visualize the presence (or not) of overlap between the $\rho_+$ and $\rho_-$ regions. In particular, it is clear that starting from P2, a very weak spatial proximity between the donor and the acceptor units is computed at PBE0 level.

More quantitatively, starting from P2, $D_{CT}$ becomes much larger than *H* thus pointing out the presence of a through-space CT, which, as reported in literature, could introduce artifacts in computed transitions when using TD-DFT in conjunction with nonasymptotically corrected functionals.[19−27]

## 5. CT INDEXES AND PERFORMANCE OF DIFFERENT FUNCTIONALS: A DIAGNOSTIC TOOL?

In order to clarify if the previously defined indexes can also be used as a diagnostic tool for the functional behavior in the reproduction of CT excitations, the first five transitions for systems P1−P4 were computed at different levels of theory, namely at TD-DFT (using the PBE, PBE0, LC-PBE functionals) and post-HF (CIS) levels.

In this context, it should be noted that although the origin of the failure of standard functionals in the description of CT excited state has been largely debated, explained, and pointed out, for the time being, practically only one efficient diagnostic index can be found in literature. This index ($\Lambda$), introduced by Tozer in 2008[37] and varying between 0 and 1, defines the spatial overlap between orbitals involved in a given electronic excitation computed using a single reference formalism (TD-DFT or CIS, for instance). Whenever the overlap is small, a through-space CT is predicted, and thus a significant error is expected when using standard GGA or hybrid functionals. Several papers by Tozer and collaborators[37−39] have confirmed the validity of such a diagnostic index, applying it to different molecular systems. As a general conclusion it seems that for transitions characterized by a small $\Lambda$, both standard GGA and hybrid functionals will yield extremely large errors. Indeed, $\Lambda$ alone, contrary to $D_{CT}$, cannot be used to identify if a given transition is a CT one or not, since CT excitations with substantial overlap will both be correctly predicted at the TD-DFT level and give a large $\Lambda$.[37−39]

Although our index is not aimed at being a quantitatively diagnostic tool, its first aim being related to the definition of the spatial extent and magnitude of a CT transition, here we would like to test if $D_{CT}$ and the centroids already both could be used to screen the CT character and as a first indicator of TD-DFT failures, at no extra computational cost.

To this end, the transition energies, oscillator strengths, and character of the first five transitions computed at different levels of theory are compared and collected in Table 4. The CT indexes of selected transitions, discussed in the text and graphically depicted in Figure 5, are reported in Table 5.

From the data reported in Table 4 several points concerning functional performances could be clearly derived. In particular, for P1 all methods provide a reasonable description of both the transition energies and their character. At all levels of theory, the most intense transition, the first one, corresponds to a CT excitation from the $NH_2$ to $NO_2$ groups (in the following noted as NN), with computed energies ranging from 406 (PBE) to 306 nm (CIS), the best agreement with experiment being obtained at PBE0 level (360 versus 372 nm experimentally determined).

From the analysis of the CT indexes reported in Table 5, it is also clear that for P1 all levels of theory predict a CT transition with substantial overlap between the centroids of charge representing the zones of increase and decrease of electron density upon excitation, with the computed value of $D_{CT}$ being very close to the *H* value.

This means that for P1, this intense transition, although having a CT character, is indeed not a through-space one, and it is

**Table 4. Computed Transition Energies (in nm), Oscillator Strengths, and Character for the P*n* Class of Compounds ($n = 1-4$)[a]**

| | PBE | | | | PBE0 | | | | LC-PBE | | | | CIS | | |
|---|---|---|---|---|---|---|---|---|---|---|---|---|---|---|---|
| *n* | $\lambda$ | *f* | type | *n* | $\lambda$ | *f* | type | *n* | $\lambda$ | *f* | type | *n* | $\lambda$ | *f* | type |
| | | | | | | | | **P1** | | | | | | | |
| 1 | 406 | 0.55 | NN | 1 | 362 | 0.65 | NN | 1 | 312 | 0.75 | NN | 1 | 306 | 1.10 | NN |
| 2 | 349 | 0.00 | $NO_2$ | 2 | 315 | 0.00 | $NO_2$ | 2 | 303 | 0.00 | $NO_2$ | 2 | 237 | 0.00 | $NO_2$ |
| 3 | 323 | 0.01 | PN | 3 | 282 | 0.01 | PN | 3 | 259 | 0.01 | $NO_2$ | 3 | 226 | 0.01 | PN |
| 4 | 288 | 0.00 | $NO_2$ | 4 | 267 | 0.00 | $NO_2$ | 4 | 248 | 0.01 | – | 4 | 218 | 0.00 | – |
| 5 | 280 | 0.06 | NP | 5 | 253 | 0.11 | NP | 5 | 215 | 0.14 | – | 5 | 208 | 1.14 | – |
| | | | | | | | | **P2** | | | | | | | |
| 1 | 641 | 0.49 | NN | 1 | 460 | 0.69 | NN | 1 | 312 | 1.09 | NN | 1 | 312 | 1.57 | NN |
| 2 | 403 | 0.01 | PN | 2 | 319 | 0.00 | $NO_2$ | 2 | 305 | 0.09 | $NO_2$ | 2 | 241 | 0.00 | $NO_2$ |
| 3 | 356 | 0.00 | $NO_2$ | 3 | 303 | 0.01 | PN | 3 | 265 | 0.00 | $NO_2$ | 3 | 240 | 0.71 | – |
| 4 | 348 | 0.01 | – | 4 | 298 | 0.03 | PN | 4 | 253 | 0.08 | – | 4 | 234 | 0.06 | – |
| 5 | 342 | 0.01 | NN | 5 | 279 | 0.01 | NN | 5 | 250 | 0.01 | – | 5 | 226 | 0.01 | – |
| | | | | | | | | **P3** | | | | | | | |
| 1 | 839 | 0.28 | NN | 1 | 483 | 0.54 | NN | 1 | 306 | 0.08 | $NO_2$ | 1 | 303 | 2.03 | PN/NN |
| 2 | 440 | 0.00 | PN | 2 | 334 | 0.52 | PN | 2 | 299 | 1.64 | NN/PN | 2 | 255 | 0.06 | – |
| 3 | 439 | 0.42 | PN | 3 | 319 | 0.03 | $NO_2$ | 3 | 266 | 0.01 | $NO_2$ | 3 | 242 | 0.00 | $NO_2$ |
| 4 | 414 | 0.02 | PN | 4 | 308 | 0.56 | NP | 4 | 253 | 0.07 | NN/PN | 4 | 242 | 1.16 | – |
| 5 | 384 | 0.44 | NN | 5 | 306 | 0.00 | PN | 5 | 253 | 0.05 | – | 5 | 240 | 0.01 | – |
| | | | | | | | | **P4** | | | | | | | |
| 1 | 940 | 0.13 | NN | 1 | 478 | 0.38 | NN | 1 | 305 | 0.02 | $NO_2$ | 1 | 298 | 2.44 | PN |
| 2 | 526 | 0.35 | PN | 2 | 371 | 0.66 | PN | 2 | 295 | 2.25 | PN | 2 | 271 | 0.18 | – |
| 3 | 456 | 0.00 | PN | 3 | 332 | 0.88 | NP | 3 | 266 | 0.00 | $NO_2$ | 3 | 242 | 0.00 | $NO_2$ |
| 4 | 437 | 0.00 | PN | 4 | 319 | 0.00 | $NO_2$ | 4 | 265 | 0.17 | NN | 4 | 242 | 1.12 | – |
| 5 | 436 | 0.54 | NP | 5 | 304 | 0.00 | PN | 5 | 253 | 0.07 | – | 5 | 240 | 0.27 | – |

[a] The following notation is used: NN = $NH_2$ to $NO_2$ CT; $NO_2$ = $NO_2$ centered excitation; PN = phenyl to $NO_2$ excitation; NP = $NH_2$ to phenyl excitation; – = $\pi-\pi^*$ excitation.

**Table 5. Computed CT indexes for P*n* systems ($n = 1$ to 5) for selected transitions at different level of theory. Experimental values from ref.[16] $\lambda$ is nm and other indexes are in Å**

| | P1 | | | | P2 | | | | P3 | | | | P4 | | | |
|---|---|---|---|---|---|---|---|---|---|---|---|---|---|---|---|---|
| | $\lambda$ | $D_{CT}$ | *H* | *t* | $\lambda$ | $D_{CT}$ | *H* | *t* | $\lambda$ | $D_{CT}$ | *H* | *t* | $\lambda$ | $D_{CT}$ | *H* | *t* |
| PBE | 406 | 2.5 | 2.0 | 0.5 | 641 | 5.0 | 3.2 | 2.8 | 839 | 7.7 | 4.3 | 3.4 | 940 | 10.2 | 5.5 | 4.7 |
| | | | | | | | | | 439 | 7.1 | 4.0 | 3.1 | 526 | 7.8 | 4.8 | 3.0 |
| PBE0 | 362 | 2.6 | 2.0 | 0.6 | 460 | 5.0 | 3.1 | 2.9 | 483 | 5.9 | 4.0 | 1.9 | 478 | 9.5 | 5.5 | 4.0 |
| | | | | | | | | | 334 | 4.6 | 3.0 | 1.6 | 371 | 7.6 | 5.2 | 2.4 |
| LC-PBE | 312 | 2.5 | 2.0 | 0.5 | 312 | 3.7 | 3.2 | 0.5 | 299 | 3.8 | 4.2 | −0.4 | 295 | 3.4 | 5.0 | −1.6 |
| CIS | 306 | 2.1 | 2.0 | 0.1 | 312 | 3.0 | 3.0 | 0.0 | 303 | 3.0 | 5.1 | −2.1 | 298 | 2.6 | $5.4_5$ | $2.8_5$ |
| expt | 372 | | | | 377 | | | | 358 | | | | 340 | | | |

therefore expected to be well predicted using standard GGA or hybrid functional, as it is in the present case. The computed centroids (graphically depicted in Figure 5) provide a simple pictorial representation of this concept.

By analysis of Table 4 it could also be noted that, starting from P2, a clearly different behavior of PBE and PBE0 with respect to LC-PBE and CIS is observed. In particular, for P2, although all the approaches predict a NN type excitation, while PBE and PBE0 predict a significant decrease in transition energies going from P1 to P2 (of the order of 1.12 and 0.73 eV for PBE and PBE0, respectively), this energy is computed as almost constant in the case of CIS and LC-PBE, in better agreement with the experimental trend.

The absolute error in transition energy computed for P2 at both PBE and PBE0 level is indeed extremely large (1.36 and 0.59 eV, respectively) when compared to their standard performances for organic molecules.[17]

The situation gets even worst when going to P3 and P4. Again, not only the transition energy computed at PBE and PBE0 levels

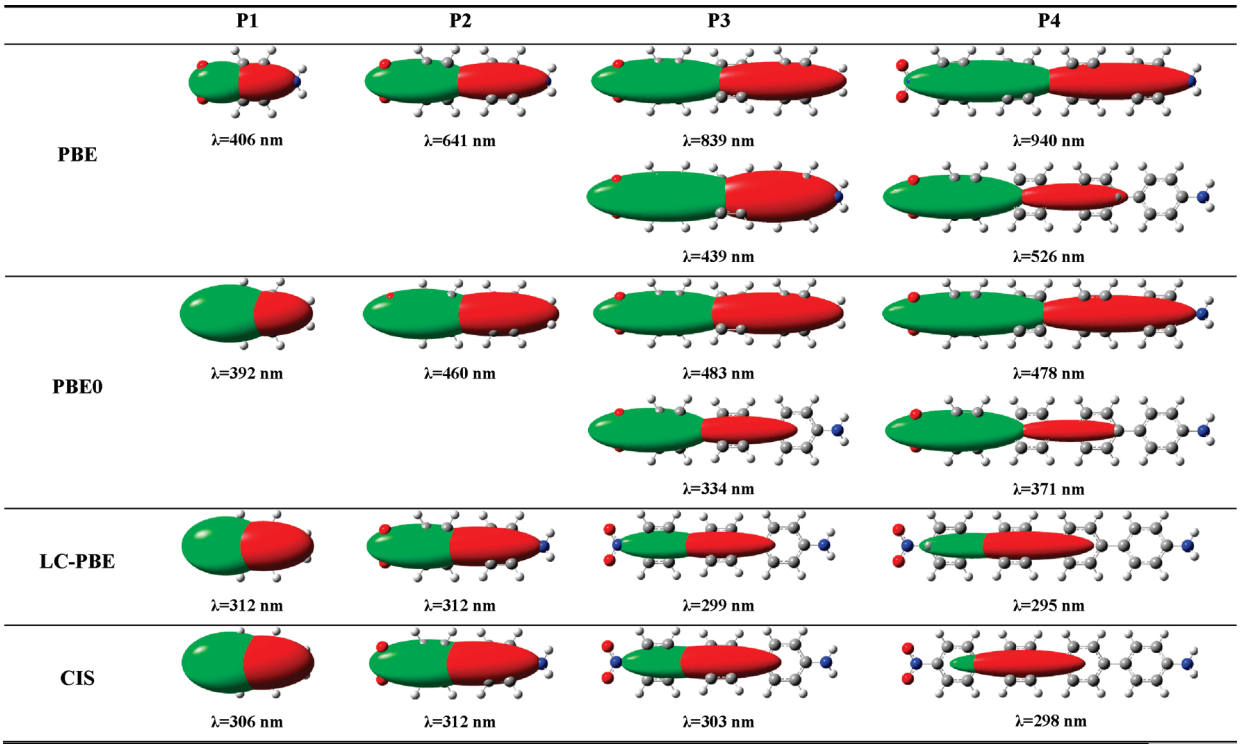


**Figure 5.** Computed transition wavelength and corresponding centroids for the highlighted transitions of Table 4 (isocontour value 0.001 au).

decreases with the increase of the length of the bridge, contrary to LC-PBE and CIS, which show a constant or slightly increasing energy in qualitative agreement with experimental data, but also and more severely the character of the most intense transition changes as a function of the method considered. In particular, while at CIS and LC-PBE levels, a CT excitation showing a significant contribution on the phenyl group linked to the $NO_2$ group is found (PN/NN), PBE and PBE0 still predict a full CT excitation from the donor to the acceptor (NN-type) at very low energies (839 and 483 nm for P3 and 940 and 478 nm for P4) and a second excitation, of PN-type, occurring at higher energies (439 and 334 nm for P3 and 526 and 371 nm for P4). These two transitions are both intense although, increasing $n$, the PN transition gains in intensity with respect to the, lower in energy, NN one.

As a consequence, going from P1 to P4, the CT length ($D_{CT}$) associated to the first transition always increases for PBE and PBE0 (and linearly correlates with the $NO_2$ to $NH_2$ distance, as discussed in Section 4.2), while it does not for CIS and LC-PBE (refer to Table 5).

In particular, for these latter two methods, a 'saturation' of the CT length is computed starting from P2, and even a slight contraction of $D_{CT}$ is computed when going from P3 to P4. This finding qualitatively correlates with the experimentally observed transition energies only slightly increasing going from P1 to P3, although neither LC-PBE nor CIS provides transitions energies in quantitative agreement with the experiment, as expected.[17,32]

Physically, it also corresponds to the fact, while the acceptor keeps localized nearby the $NO_2$ group for all systems, the donor, primarily represented by the $NH_2$ group, actually delocalizes to the phenyl groups when increasing the bridge length and when starting from a three phenyl units bridge, is actually represented only by phenyl groups, as evident from the analysis of the centroids of charge (Figure 5).

Only at LC-PBE and CIS levels, going from P2 to P4, also the acceptor moiety shifts from the $NO_2$ group to the phenyl linked to it, thus finally giving rise to a very short-range CT transition (Figure 5). Analysis of the centroid allows also to easily visualize the tendency toward delocalization of GGA functional (larger centroids) with respect to the more localized character of hybrid and range-separated functionals.

As a consequence, analyzing the CT indexes computed at different levels of theory (Table 5), it could be noted that at both the CIS and LC-PBE levels, the CT length ($D_{CT}$) only slightly increases going from P1 to P2, keeping constant from P2 to P3 and slightly contracting while passing from P3 to P4. This behavior closely parallels the experimentally observed transition energies. As a consequence, for all systems the CT length is computed between 2.5 Å (P1) and 3.8 Å (P3) at LC-PBE level and between 2.1 Å (P1) and 3.0 Å (P3) at CIS level.

On the other hand, PBE and PBE0 predict a much larger $D_{CT}$ associated to the first intense transitions for all systems, except P1 for which all methods yield the same picture.

Indeed, it could be noticed that already starting from P2, both at PBE and PBE0 level for the first transition $D_{CT} \gg H$, thus implying the presence of a through-space CT. Not surprisingly starting from P2 the computed transition energies associated with the first electronic transition do not follow both the experimental and the LC-PBE or CIS trends.

The difference between $D_{CT}$ and $H$, noted $t$ (eq 14 and Table 5), seems thus a reasonable diagnostic index for TD-DFT transitions. From the data collected for the family of molecules currently investigated, a $t > 1.6$ Å points out a potentially problematic transition for standard GGA and hybrid functionals.

Of note this rule of thumb, derived from the analysis of the first transition, also applies to the second intense transition computed

at PBE and PBE0 level for P3 and P4, which indeed has the same PN character as that predicted at LC-PBE or CIS. Indeed, only in the case of P3 computed at PBE0 level, the $t$ criteria is satisfied, thus pointing out that for P4, both PBE and PBE0 should in principle provide very large errors also for the second transition, which is actually the case.

## 6. CONCLUSIONS

A new simple index ($D_{CT}$) aimed at giving a measure of the length of the electron transfer associated to an electronic transition has been introduced and tested on a family of push−pull molecules derived from the 1-amino-4-nitrobenzene.

The index, based only on the computed electronic density for the ground and excited states, quantifies the charge-transfer (CT) length as the distance between the barycenters of the density increment and depletion regions upon electronic excitation. As a consequence, it could be computed at any level of theory providing both ground- and excited-state densities. Clearly this index will be exactly zero for any centrosymmetric system. In such a case the index should be evaluated on the corresponding symmetry irreductible subunits.

The definition of centroids of charges associated to the density increase and depletion zones centered on the barycenters of charge previously defined allows to visualize and quantify the spatial extent of the donor and acceptor groups within a given molecular system. For this reason both $D_{CT}$ and the centroids can be of help for the design and the description of new push−pull systems at both the theoretical and the experimental levels.

Finally the possibility of using a quantity related to the overlap between the centroids (namely, $t$) has been tested as a diagnostic tool to point out the pathological behavior of TD-DFT for the description of through-space CT transitions. From the results obtained for the classes of molecule analyzed it seems that $t$ can be used to highlight the through-space character of a given electronic transitions and, thus, as a first warning for possible TD-DFT failures.

As a consequence, the combined uses of $D_{CT}$ and $t$ will allow to define the character (CT or not) and the magnitude (in term of spatial extent, i.e., the length of transition) of a given transition and to be a first indicator of eventual CT pathologic cases for DFT. Further work is in progress in this direction in our group.

## ■ ASSOCIATED CONTENT

**Supporting Information.** Optimized structures of P$n$ ($n$ = 1−5) systems. This material is available free of charge via the Internet at http://pubs.acs.org.

## ■ AUTHOR INFORMATION

### Corresponding Author

*E-mail: tangui-le-bahers@chimie-paristech.fr; ilaria-ciofini@chimie-paristech.fr.

## ■ ACKNOWLEDGMENT

Ciro A. Guido (SNS, Pisa Italy) is thanked for fruitful discussions on CT indexes. Members of the COST Action CODECS are gratefully acknowledged for constructive comments. The French National Agency for Research (ANR) is acknowledged for financial support to I.C. and C.A. in the framework of the "NEXUS project (Programme Blanc 2007, BLAN07-1-196405).

## ■ REFERENCES

(1) (a) Bureš, F.; Pytela, O.; Kivala, M.; Diederich, F. *J. Phys. Org. Chem.* **2011**, *24*, 274–281. (b) Blanchard-Desce, M.; Wortmann, R.; Lebus, S.; Lehn, J.-M.; Krämer, P. *Chem. Phys. Lett.* **1995**, *243*, 526–532. (c) Pocker, Y.; Spyridis, G. T. *J. Am. Chem. Soc.* **2002**, *124*, 7390–7394.

(2) Juris, A.; Balzani, V.; Barigelletti, F.; Belser, P.; Von Zelewsky, A. *Coord. Chem. Rev.* **1988**, *84*, 85–277.

(3) Le Bahers, T.; Pauporté, T.; Scalmani, G.; Adamo, C.; Ciofini, I. *Phys. Chem. Chem. Phys.* **2009**, *11*, 11276–11284.

(4) Ciofini, I.; Lainé, P. P.; Bedioui, F.; Adamo, C. *J. Am. Chem. Soc.* **2004**, *126*, 10763–10777.

(5) Fortage, J.; Peltier, C.; Nastasi, F.; Puntoriero, F.; Tuyères, F.; Griveau, S.; Bedioui, F.; Campagna, S.; Lainé, P. P. *J. Am. Chem. Soc.* **2010**, *132*, 16700–16713.

(6) Peltier, C.; Adamo, C.; Lainé, P. P.; Campagana, S.; Punteriero, F.; Ciofini, I. *J. Phys. Chem. A* **2010**, *114*, 8434–8443.

(7) Robb, M. A.; Haines, W. J.; Csizmadia, I. G. *J. Am. Chem. Soc.* **1973**, *95*, 42–48.

(8) Amhadi, G. R.; Røeggen, I. *Theor. Chem. Acc.* **1997**, *97*, 41–46.

(9) Barone, V.; Adamo, C. *J. Chem. Phys.* **1999**, *110*, 6158–6170.

(10) Krishnan, R.; Binkley, J. S.; Pople, J. A. *J. Chem. Phys.* **1980**, *72*, 650–654.

(11) Frisch, M. J.; Trucks, G. W.; Schlegel, H. B.; Scuseria, G. E.; Robb, M. A.; Cheeseman, J. R.; Scalmani, G.; Barone, V.; Mennucci, B.; Petersson, G. A.; Nakatsuji, H.; Caricato, M.; Li, X.; Hratchian, H. P.; Izmaylov, A. F.; Bloino, J.; Zheng, G.; Sonnenberg, J. L.; Hada, M.; Ehara, M.; Toyota, K.; Fukuda, R.; Hasegawa, J.; Ishida, M.; Nakajima, T.; Honda, Y.; Kitao, O.; Nakai, H.; Vreven, T.; Montgomery, J. A., Jr.; Peralta, J. E.; Ogliaro, F.; Bearpark, M.; Heyd, J. J.; Brothers, E.; Kudin, K. N.; Staroverov, V. N.; Kobayashi, R.; Normand, J.; Raghavachari, K.; Rendell, A.; Burant, J. C.; Iyengar, S. S.; Tomasi, J.; Cossi, M.; Rega, N.; Millam, N. J.; Klene, M.; Knox, J. E.; Cross, J. B.; Bakken, V.; Adamo, C.; Jaramillo, J.; Gomperts, R.; Stratmann, R. E.; Yazyev, O.; Austin, A. J.; Cammi, R.; Pomelli, C.; Ochterski, J. W.; Martin, R. L.; Morokuma, K.; Zakrzewski, V. G.; Voth, G. A.; Salvador, P.; Dannenberg, J. J.; Dapprich, S.; Daniels, A. D.; Farkas, Ö.; Foresman, J. B.; Ortiz, J. V.; Cioslowski, J.; Fox, D. J. *Gaussian 09*, revision A.02; Gaussian, Inc.: Wallingford, CT, 2009.

(12) Miertuš, S.; Scrocco, E.; Tomasi, J. *Chem. Phys.* **1981**, *55*, 117–129.

(13) Barone, V.; Cossi, M. *J. Phys. Chem. A* **1998**, *102*, 1995–2001.

(14) Perdew, J. P.; Burke, K.; Ernzerhof, M. *Phys. Rev. Lett.* **1960**, *77*, 3865–3868.

(15) Iikura, H.; Tsuneda, T.; Yanai, T.; Hirao, K. *J. Chem. Phys.* **2001**, *115*, 3540–3544.

(16) Berry, R. W. H.; Brocklehurst, P.; Burawoy, A. *Tetrahedron* **1960**, *10*, 109–117.

(17) Jacquemin, D.; Perpète, E.; Ciofini, I.; Adamo, C. *Acc. Chem. Res.* **2009**, *42*, 326–334.

(18) Tozer, D. *J. Chem. Phys.* **2003**, *199*, 12697–12699.

(19) Tozer, D.; Amos, R. D.; Handy, N. C.; Roos, B. O.; Serran-Andres, L. *Mol. Phys.* **1999**, *97*, 859–868.

(20) Fabian, J. *Theor. Chem. Acc.* **2001**, *106*, 199–217.

(21) Dreuw, A.; Head-Gordon, M. *J. Am. Chem. Soc.* **2004**, *126*, 4007–4016.

(22) Dreuw, A.; Head-Gordon, M. *Chem. Rev.* **2005**, *105*, 4009–4037.

(23) Hieringer, W.; Görling, A. *Chem. Phys. Lett.* **2006**, *419*, 557–562.

(24) Dreuw, A.; Head-Gordon, M. *Chem. Phys. Lett.* **2006**, *426*, 231–233.

(25) Kummel, S.; Kronik, S. *Rev. Mod. Phys.* **2008**, *80*, 3–60.

(26) Cohen, A. J.; Mori-Sanchez, P.; Yang, W. T. *Science* **2008**, *321*, 792–794.

(27) Dreuw, A.; Weisman, J. L.; Head-Gordon, M. *J. Chem. Phys.* **2003**, *119*, 2943–2946.

(28) Ziegler, T.; Krykunov, M. *J. Chem. Phys.* **2010**, *133*, 074104.
(29) Ziegler, T.; Seth, M.; Krykunov, M.; Autschbach, J.; Wang, F. *J. Mol. Struct. THEOCHEM* **2009**, *914*, 106–109.
(30) Ziegler, T.; Seth, M.; Krykunov, M.; Autschbach, J. *J. Chem. Phys.* **2008**, *129*, 184114.
(31) Görling, A.; Ipatov, A.; Götz, A. W.; Hesselmann, A. *Z. Phys. Chem.* **2010**, *224*, 03–04.
(32) Jacquemin, D.; Perpète, E. A.; Scuseria, G. E.; Ciofini, I.; Adamo, C. *J. Chem. Theory Comput.* **2008**, *4*, 123–135.
(33) Stein, T.; Kronik, L.; Baer, R. *J. Am. Chem. Soc.* **2009**, *131*, 2818–2820.
(34) Livshits, E; Baer, R. *Phys. Chem. Chem. Phys.* **2007**, *9*, 2932–2941.
(35) Tawada, Y.; Tsuneda, T.; Yanagisawa, S.; Yanai, T.; Hirao, K. *J. Chem. Phys.* **2004**, *120*, 8425–8433.
(36) Rohrdanz, M. A.; Herbert, J. M. *J. Chem. Phys.* **2008**, *129*, 034107.
(37) Peach, M. J. G.; Benfield, P.; Helgaker, T.; Tozer, D. J. *J. Chem. Phys.* **2008**, *128*, 044118.
(38) Peach, M. J. G.; Tozer, D. J. *J. Mol. Struc.: THEOCHEM* **2009**, *914*, 110–114.
(39) Peach, M. J. G.; Le Sueur, C. R.; Ruud, K.; Guillaume, M.; Tozer, D. J. *Phys. Chem. Chem. Phys.* **2009**, *11*, 4465–4470.